

# Achieving Heisenberg limit of metrology via measurement on ancillary qubit

Peng Chen<sup>1</sup> and Jun Jing<sup>1,\*</sup>

<sup>1</sup>*School of Physics, Zhejiang University, Hangzhou 310027, Zhejiang, China*

We propose a measurement-based quantum metrology protocol by coupling the probe (a spin ensemble) to an ancillary qubit. The key element is to use the optimized joint evolution time and the unconditional measurement on the ancillary qubit to bring the probe system from an eigenstate of a collective angular momentum operator  $|j, m\rangle$  to a superposed state  $(|j, m\rangle + |j, -m\rangle)/\sqrt{2}$ . With synchronous parametric encoding and unconditional measurement, the quantum Fisher information about the phase encoded in the probe system can exactly attain the Heisenberg scaling  $N^2$  with respect to the probe size (spin number)  $N$  upon optimized initial states. The quadratic scaling behavior is not sensitive to the imprecise control over the joint evolution time and the time delay between encoding and measurement. The classical Fisher information of the spin ensemble is found to saturate with its quantum counterpart, irrespective of the idle evolution time after the parametric encoding. We suggest that both GHZ-like state and nonlinear Hamiltonian are not necessary resources for metrology precision since in our protocol even thermal states hold an asymptotic quadratic scaling.

## I. INTRODUCTION

Quantum metrology aims to push the measurement precision to the ultimate limit constrained by the intrinsic uncertainty of quantum mechanics [1–6]. A fundamental limit of quantum metrology in uncorrelated systems is the standard quantum limit (SQL) on the errors of parameter estimation, which scales linearly with  $1/\sqrt{N}$  with  $N$  the total number of measurements. This shot-noise scaling law is essentially rooted in the central limit theorem of classical statistics [7]. If nonclassical resources [e.g., the Greenberger-Horne-Zeilinger (GHZ) state in atomic systems and the NOON state in photonic systems] are introduced to the systems, the sensitivity of quantum measurements can be enhanced and the precision limit of parameter estimation can exceed the SQL and approach the Heisenberg limit (HL), representing a scaling law inverse to the number of probe units with  $1/N$ . Realizing this enhancement with a large quantum number is an ongoing target of a wide range of potential applications including atomic clock [8, 9], gravitational wave detection [10], biological sensing [11, 12], and magnetometry [13].

In practical situations, generating GHZ-like state in multiparticle systems to improve metrology precision is a highly non-trivial task. One of the strategies for generating GHZ state is to apply the entangling gates to qubits [14–17], but the achievement is very limited. So far an 18-qubit GHZ state has been generated on a quantum processor [14]. A large-scale GHZ state can be generated using the collective-spin one-axis twisting (OAT) Hamiltonian  $H_{\text{OAT}} = \chi J_z^2$  [18] on the separable spin coherent states, but the required duration  $\chi t = \pi/2$  is quite long, setting obstacles for generation due to decoherence and particle loss [19–22]. Measurement and postselection can be used to reduce the evolution time at the cost of

the success probability [23]. It is shown that by adding a turning term  $\propto J_x$  to an OAT Hamiltonian, a many-particle entangled state that resembles GHZ state can be obtained in a shorter timescale with  $\chi t = \pi/4$  [23, 24], but it differs from the ideal GHZ state due to its wide distribution on the Dicke state basis.

We introduce a measurement-based metrology protocol to estimate the phase parameter  $\theta$  imprinted to the probe system (a spin ensemble) during a spin rotation. It is based on the well prepared ancillary qubit and probe, their joint evolution on mutual interaction, and the unconditional measurement on qubit. After an optimal period of joint evolution and measurement, the probe can evolve from a collective angular momentum eigenstate  $|j, m\rangle$  to a superposed state  $(|j, m\rangle + |j, -m\rangle)/\sqrt{2}$ . When the initial probe state is a polarized state  $|j, j\rangle$ , the ideal GHZ state can be generated. If the to-be-estimated parameter  $\theta$  is encoded to the probe state at the same time of measurement, the quantum Fisher information (QFI) about  $\theta$  can approach the Heisenberg scaling  $N^2$  in terms of the total spin number  $N$ . It is interesting to find that an asymptotic Heisenberg-scaling behavior about the metrology precision holds even when the probe is prepared as a thermal state. This scaling behavior is not sensitive to the imprecise control over the joint evolution time and the time delay between the parametric encoding and the measurement on the ancillary qubit. Moreover, the classical Fisher information (CFI) of our protocol is found to be coincident with the QFI by the projective measurements on the probe system, irrespective of the idle evolution after all the operations.

The rest of this work is structured as follows. In Sec. II, we briefly recall the classical Fisher information and its quantum counterpart, distinguishing the critical role of probe state played in the estimation theory. In Sec. III, we describe the circuit model of our metrology protocol assisted by the unconditional measurement on the ancillary qubit. In Sec. IV, we investigate the parametric conditions and initial states of the probe system for attaining the Heisenberg limit in metrology precision. In

---

\* Email address: jingjun@zju.edu.cn

Sec. V, we discuss the sensitivity of our metrology protocol to the imprecise controls over the evolution time and the time delay between encoding and measurement on qubit. In Sec. VI, we calculate CFI in our protocol as the amount of extractable information from the probability distribution of the output state of the probe system upon projective measurements. The entire work is summarized in Sec. VII.

## II. ESSENTIAL ROLE OF PROBE STATE

The Fisher information and the Cramér-Rao bound are foundational concepts in quantifying the limits of precision in parameter estimation. These concepts are pivotal in both classical and quantum domains, offering insight into the optimal accuracy achievable in the noise-free situation.

In the classical domain, the classical Fisher information provides a measure about the sensitivity of the probability distribution of the system state to the changes in parameters. Assuming that  $\{p(x_i|\theta), \theta \in \mathbb{R}\}_{i=1}^N$  is the probability density conditioned on the fixed value of the phase parameter  $\theta$  with the measurement outcomes  $\{x_i\}$ , the Fisher information  $F_C$  is defined as [25]

$$F_C = \sum_i \frac{[\partial_\theta p(x_i|\theta)]^2}{p(x_i|\theta)}, \quad (1)$$

where  $\partial_\theta \equiv \partial/\partial\theta$ . When the observable  $\hat{X}$  is a continuous variable, the summation in Eq. (1) should be replaced by an integral.

The quantum analog of the Fisher information is formally generalized from Eq. (1) and defined as

$$F_Q = \text{Tr}(\rho_\theta L_\theta^2) \quad (2)$$

in terms of the symmetric logarithmic derivative (SLD) operator  $L_\theta$ , which is a Hermitian operator defined as

$$\partial_\theta \rho_\theta = \frac{1}{2}(\rho_\theta L_\theta + L_\theta \rho_\theta). \quad (3)$$

By diagonalizing the density matrix as

$$\rho_\theta = \sum_{i=1}^d p_i |\psi_i(\theta)\rangle \langle \psi_i(\theta)|, \quad (4)$$

with  $p_i \geq 0$  and  $\sum_{i=1}^d p_i = 1$ , the elements of the SLD operator are completely defined under the condition  $p_i + p_j \neq 0$ . Therefore, Eq. (2) can be expressed as [26]

$$F_Q = \sum_{i=1}^d 4p_i \langle \partial_\theta \psi_i(\theta) | \partial_\theta \psi_i(\theta) \rangle - \sum_{i,j=1}^d \frac{8p_i p_j}{p_i + p_j} |\langle \psi_i(\theta) | \partial_\theta \psi_j(\theta) \rangle|^2. \quad (5)$$

Consider a general unitary parametrization process

$$U_\theta^\dagger U_\theta = \mathcal{I}^d, \quad (6)$$

with  $\mathcal{I}^d$  being the identity matrix of  $d$  dimensions, the density matrix in Eq. (4) becomes

$$\rho_\theta = U_\theta \rho_0 U_\theta^\dagger = U_\theta \left( \sum_{i=1}^d p_i |\psi_i\rangle \langle \psi_i| \right) U_\theta^\dagger, \quad (7)$$

where

$$\rho_0 = \sum_{i=1}^d p_i |\psi_i\rangle \langle \psi_i| \quad (8)$$

is the spectral decomposition of the initial state before parametric encoding. By Eq. (7), Eq. (5) reduces to [26–29]

$$F_Q = \sum_{i=1}^d 4p_i \langle \psi_i | \mathcal{H}^2 | \psi_i \rangle - \sum_{i,j=1}^d \frac{8p_i p_j}{p_i + p_j} |\langle \psi_i | \mathcal{H} | \psi_j \rangle|^2 \quad (9)$$

with the effective phase generator  $\mathcal{H} \equiv iU_\theta^\dagger (\partial_\theta U_\theta)$ . Note even if the parametrization process  $U_\theta$  is non-unitary [30], Eq. (9) still holds if the initial state is a pure state or its spectral decomposition satisfies the condition

$$\langle \psi_i | U_\theta^\dagger U_\theta | \psi_j \rangle = 0 \quad (10)$$

for all  $i \neq j$ .

For a pure initial state  $\rho_0 = |\psi\rangle \langle \psi|$ , the quantum Fisher information in Eq. (9) is reduced to

$$F_Q = 4\langle \psi | \mathcal{H}^2 | \psi \rangle - 4|\langle \psi | \mathcal{H} | \psi \rangle|^2. \quad (11)$$

One can find that the variance of the phase generator  $\mathcal{H}$  becomes maximized when the initial state  $|\psi\rangle$  is an equally weighted superposition of the eigenvectors  $|\lambda_{\max}\rangle$  and  $|\lambda_{\min}\rangle$  with  $\lambda_{\max}$  and  $\lambda_{\min}$  the maximum and minimum eigenvalues of  $\mathcal{H}$ , respectively [31, 32], i.e.,

$$|\psi\rangle = \frac{1}{\sqrt{2}}(|\lambda_{\max}\rangle + e^{i\phi}|\lambda_{\min}\rangle), \quad (12)$$

where  $\phi$  is an arbitrary relative phase. Thus the maximal QFI is [32]

$$F_Q^{\max} = (\lambda_{\max} - \lambda_{\min})^2. \quad (13)$$

An important observation is that  $|\psi\rangle$  can be a maximal entangled state for a many-body system, e.g., GHZ state and NOON state. For a parametric encoding about the  $x$ -axis, i.e.,  $\mathcal{H} = J_x$  of a high-spin system, the relevant GHZ state is

$$|\text{GHZ}\rangle = \frac{1}{\sqrt{2}}(\mathcal{I}^{N+1} + e^{-i\phi} e^{i\pi J_z})|j, j\rangle_x, \quad (14)$$

where  $|j, m\rangle_x$  is the eigenstate of the collective spin operators  $J_x$  with eigenvalue  $m$  and  $N = 2j$ . It suggests that the superposed state in Eq. (12) with maximally departed distribution in eigenspace, e.g., the GHZ state, can be generated by constructing two distinct evolution paths. This idea can be carried out through the measurement on the ancillary qubit in this work, by which a polarised state can be transformed to be a GHZ state.

### III. METROLOGY WITH ANCILLARY QUBIT

In this paper, we consider a metrology model consisting of a high-spin probe (spin ensemble) and an ancillary spin-1/2. The full Hamiltonian including the free part  $H_0$  and the interaction part  $H_I$  reads ( $\hbar \equiv 1$ )

$$H = H_0 + H_I = \omega_P J_z + \omega_A \sigma_z + g J_z \sigma_z, \quad (15)$$

where  $J_\alpha = \sum_{k=1}^N \sigma_\alpha^k/2$ ,  $\alpha = x, y, z$ , denotes the collective spin operator with  $\sigma_\alpha^k$  the  $\alpha$ -component of Pauli matrix of the  $k$ th probe spin,  $\omega_P$  and  $\omega_A$  represent the energy splitting of the probe spin and the ancillary spin, respectively, and  $g$  is the coupling strength between the two components.

The free Hamiltonian and the interaction Hamiltonian in Eq. (15) are feasible in various experiments. The interaction Hamiltonian can be realized by the atoms interacting with the photon mode due to a quantum non-demolition interaction [33, 34], where  $J_z$  is the sum of the total angular momentum of individual atoms and  $\sigma_z$  denotes the Stokes operator associated with the distinction between the number operators of the photons polarized along orthogonal bases. The Hamiltonian can also be realized by two cavities containing two-component Bose-Einstein condensates coupled by cavity quantum electrodynamics [35, 36], where the operators  $J_z$  and  $\sigma_z$  correspond to the Schwinger boson operators  $a^\dagger a - b^\dagger b$  in the relevant cavities with  $a^\dagger$  and  $b^\dagger$  being bosonic creation operators for two orthogonal quantum states. In quantum dots [37],  $J_z$  and  $\sigma_z$  describe the nuclear spins and the electron spin, respectively, and  $g J_z \sigma_z$  describes the hyperfine interaction.

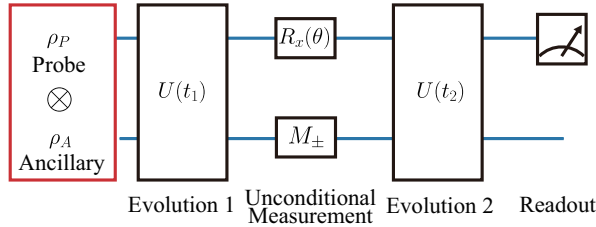


FIG. 1. Circuit model of our measurement-based metrology. Evolution 1 and 2 denote the free joint unitary evolution  $U(t_1)$  and  $U(t_2)$ , respectively, in between which the unconditional measurement  $M_\pm$  in the basis of  $\sigma_x$  is performed on the ancillary qubit and meanwhile a to-be-estimated parameter  $\theta$  is encoded into the probe state via a unitary rotation  $R_x(\theta)$  about the  $J_x$  direction. The output state is determined by projective measurements on the probe state.

The probe spin ensemble and the ancillary qubit are initially separable, i.e., the input state of the full system is a product state  $\rho_P \otimes \rho_A$  as indicated by Fig. 1. The whole evolution operator of the circuit can be described by

$$U_{\theta, \pm} = U(t_2) R_x(\theta) M_\pm U(t_1) = e^{-iHt_2} e^{-i\theta J_x} |\pm\rangle \langle \pm| e^{-iHt_1}, \quad (16)$$

where  $|\pm\rangle = (|e\rangle \pm |g\rangle)/\sqrt{2}$  is the eigenvector of  $\sigma_x$ . Here  $|g\rangle$  and  $|e\rangle$  denote the ground and excited states of the ancillary spin, respectively. During Evolution 1 and Evolution 2, the probe system and the ancillary qubit experience a joint time evolution lasting  $t_1$  and  $t_2$ , respectively. On the stage of Unconditional Measurement, the projection  $M_\pm = |\pm\rangle \langle \pm|$  is performed on the ancillary qubit. At the same time, the phase parameter  $\theta$  is imprinted to the probe system (a spin ensemble) by a spin rotation  $R_x(\theta) = \exp(-i\theta J_x)$  of a negligible duration (alternatively, the interaction Hamiltonian in between the two evolutions can be temporarily switched off). Experimentally,  $\theta$  can be accumulated during the precessing about the  $z$ -axis [38–40] induced by a certain interaction between the probe and a to-be-measured system. Then the rotation about the  $x$ -axis could be realized by a sequence of  $R_x(\theta) = R_y(\pi/2) R_z(\theta) R_y(-\pi/2)$ , where  $R_y(\pm\pi/2)$  indicates the  $\pi/2$  pulse about  $y$ -axis. On the last stage of the circuit, projective measurements are performed on the output state about the probe system  $\rho_\pm(\theta) \equiv \text{Tr}_A[U_{\theta, \pm} \rho_P \otimes \rho_A U_{\theta, \pm}^\dagger]$  with  $\text{Tr}_A$  the partial trace over the ancillary qubit, whose probability distribution can be used to infer the classical Fisher information about the estimated parameter  $\theta$ .

### IV. PREPARATION OF A STATE WITH MAXIMALLY DEPARTED DISTRIBUTION

The key insight underlying our protocol is to use the free joint unitary evolution for Evolution 1 and the unconditional measurement  $M_\pm$  to prepare a state with a maximally departed distribution in state space. Irrespective to the outcome of the measurement, the whole process will continue and each unravelling of the probe is usually a maximally entangled state when it starts from a pure state. Suppose the probe system and the ancillary qubit are prepared as pure states  $\rho_P = |\psi\rangle \langle \psi|$  and  $\rho_A = |\varphi\rangle \langle \varphi|$ . After the unitary evolution  $U(t_1)$  and a measurement on the ancillary qubit in the  $\sigma_x$  basis, the unnormalized output state reads

$$|\Psi_\pm\rangle = M_\pm U(t_1) |\psi\rangle \otimes |\varphi\rangle = \langle \pm | e^{-iHt_1} |\varphi\rangle |\psi\rangle \otimes |\pm\rangle, \quad (17)$$

where the subscripts  $\pm$  indicate the measurement results. Using Eq. (15), the evolution operator of Evolution 1 can be expressed as

$$e^{-iHt_1} = \frac{1}{2} \exp\{-i[\omega_A + (\omega_P + g)J_z]t_1\} \times [P_+(t_1) \otimes |+\rangle \langle +| + P_-(t_1) \otimes |+\rangle \langle -| + P_+(t_1) \otimes |-\rangle \langle -| + P_-(t_1) \otimes |-\rangle \langle +|], \quad (18)$$

with  $P_\pm(t) = \mathcal{I}^{N+1} \pm e^{2i(\omega_A + gJ_z)t}$ , where  $N = 2j$  is the total spin number of the probe ensemble. It is found that the evolution operator can be considered as the sum of two evolution paths  $P_\pm$  for the probe, which can be unraveled upon choosing a proper state of the ancillary

qubit, i.e.,

$$|\varphi\rangle_{\text{opt}} = |\pm\rangle. \quad (19)$$

Without loss of generality, we first consider the initial state  $|\varphi\rangle_{\text{opt}} = |+\rangle$ . Consequently, the unnormalized output state of the composite system becomes

$$\begin{aligned} |\Psi_{\pm}\rangle &= \langle \pm | e^{-iHt_1} | \varphi \rangle_{\text{opt}} | \psi \rangle \otimes | \pm \rangle \\ &= \frac{1}{2} e^{-i\omega_A t_1} (\mathcal{I}^{N+1} \pm e^{2i\omega_A t_1} e^{2igt_1 J_z}) \\ &\quad e^{-i(\omega_P + g)t_1 J_z} | \psi \rangle \otimes | \pm \rangle. \end{aligned} \quad (20)$$

One can find that Eqs. (14) and (20) share the same formation up to a global phase. It indicates that the GHZ state can be generated with a proper initial state of the probe system

$$| \psi \rangle_{\text{opt}} = | j, \pm j \rangle_{\text{opt}} = e^{i(\omega_P + g)t_{1,\text{opt}} J_z} | j, \pm j \rangle_x, \quad (21)$$

where the subscript  $x$  denotes the eigenstate of  $J_x$ , and an optimized joint-evolution time for Evolution 1,

$$t_{1,\text{opt}}(n_1) = \left( n_1 + \frac{1}{2} \right) \frac{\pi}{g} \quad (22)$$

with  $n_1$  integer. Here  $| j, m \rangle_{\text{opt}}$  with  $-j \leq m \leq j$  denote the eigenstates for the optimized collective angular momentum operator

$$\begin{aligned} J_{\text{opt}} &= e^{i(\omega_P + g)t_{1,\text{opt}} J_z} J_x e^{-i(\omega_P + g)t_{1,\text{opt}} J_z} \\ &= \cos[(\omega_P + g)t_{1,\text{opt}}] J_x - \sin[(\omega_P + g)t_{1,\text{opt}}] J_y, \end{aligned} \quad (23)$$

according to Eq. (20).

Then after the encoding  $R_x(\theta)$  and the idle evolution  $U(t_2)$  in Eq. (16), the unnormalized output state will become

$$\begin{aligned} | \Psi_{\theta, \pm} \rangle &= \frac{1}{2} e^{-i\omega_A t_{1,\text{opt}}} U(t_2) R_x(\theta) \\ &\quad (| j, j \rangle_x \pm i^N e^{2i\omega_A t_{1,\text{opt}}} | j, -j \rangle_x) \otimes | \pm \rangle, \end{aligned} \quad (24)$$

with a probability  $\mathcal{N}_{\pm} = \langle \Psi_{\theta, \pm} | \Psi_{\theta, \pm} \rangle = 1/2$ . The probability (normalization factor) is always 50%, irrespective of the to-be-determined phase parameter  $\theta$ . Using the pure-state formula in Eq. (11), the effective QFI is found to be

$$\begin{aligned} F_{Q, \pm, \text{eff}} &= 4\mathcal{N}_{\pm} [ \langle \partial_{\theta} \Psi'_{\theta, \pm} | \partial_{\theta} \Psi'_{\theta, \pm} \rangle - | \langle \Psi'_{\theta, \pm} | \partial_{\theta} \Psi'_{\theta, \pm} \rangle |^2 ] \\ &= 4 \langle \partial_{\theta} \Psi_{\theta, \pm} | \partial_{\theta} \Psi_{\theta, \pm} \rangle = N^2/2 \end{aligned} \quad (25)$$

with the normalized state  $| \Psi'_{\theta, \pm} \rangle = | \Psi_{\theta, \pm} \rangle / \sqrt{\mathcal{N}_{\pm}}$ . Since the unconditional measurement on the ancillary qubit is free of whether the result is  $|+\rangle$  or  $|-\rangle$ , one can use the sum of the effective QFIs  $F_{Q, +, \text{eff}}$  and  $F_{Q, -, \text{eff}}$  to indicate the full QFI, i.e.,

$$F_Q = F_{Q, +, \text{eff}} + F_{Q, -, \text{eff}} = N^2. \quad (26)$$

It is therefore found that the Heisenberg scaling can be approached under proper qubit state, optimized probe

state, and optimized joint evolution time  $t_1$  before encoding and measurement.

When the ancillary qubit is prepared in another optimized state  $|\varphi\rangle_{\text{opt}} = |-\rangle$ , the composite system becomes

$$\begin{aligned} | \Psi_{\pm} \rangle &= \frac{1}{2} e^{-i\omega_A t_1} (\mathcal{I}^{N+1} \mp e^{2i\omega_A t_1} e^{2igt_1 J_z}) \\ &\quad e^{-i(\omega_P + g)t_1 J_z} | \psi \rangle \otimes | \pm \rangle, \end{aligned} \quad (27)$$

which is similar to Eq. (20). Upon the optimal conditions in Eqs. (21) and (22), one can obtain the same result as Eq. (26).

If the probe system  $\rho_P$  is initialized as a mixed state, such as  $\rho_0$  in Eq. (8), then the output state of the composite system after three stages of evolution (16) will become

$$\rho_{\theta, \pm} = U'_{\theta, \pm} \rho_0 U'^{\dagger}_{\theta, \pm} \otimes | \pm \rangle \langle \pm | \quad (28)$$

under the optimized initial state of the ancillary qubit  $|\varphi\rangle_{\text{opt}} = |+\rangle$  and the joint-evolution time in Eq. (22). Here the effective evolution operator reads

$$U'_{\theta, \pm} = e^{-iHt_2} e^{-i\theta J_z} \langle \pm | e^{-iHt_{1,\text{opt}}} | + \rangle / \sqrt{\mathcal{N}'_{\pm}} \quad (29)$$

with the normalized factor

$$\mathcal{N}'_{\pm} = \text{Tr}[\langle \pm | e^{-iHt_{1,\text{opt}}} | + \rangle \rho_0 \langle + | e^{iHt_{1,\text{opt}}} | \pm \rangle]. \quad (30)$$

The unitarity condition for the effective evolution operator is *not* always ensured unless

$$\begin{aligned} U'^{\dagger}_{\theta, \pm} U'_{\theta, \pm} &= \frac{1}{\mathcal{N}'_{\pm}} \langle + | e^{iHt_{1,\text{opt}}} | \pm \rangle \langle \pm | e^{-iHt_{1,\text{opt}}} | + \rangle \\ &= \frac{2\mathcal{I}^{N+1} \pm [e^{2i\omega_A t_{1,\text{opt}}} + (-1)^N e^{-2i\omega_A t_{1,\text{opt}}}] e^{i\pi J_z}}{2 \pm [e^{2i\omega_A t_{1,\text{opt}}} + (-1)^N e^{-2i\omega_A t_{1,\text{opt}}}] \text{Tr}[e^{i\pi J_z} \rho_0]} \\ &= \mathcal{I}^{N+1}, \end{aligned} \quad (31)$$

which is equivalent to require

$$\omega_A = \frac{N+1+2n_2}{4t_{1,\text{opt}}(n_1)} \pi, \quad (32)$$

with  $n_2$  integer. Thus the qubit frequency  $\omega_A$  has to be relevant to the optimized joint-evolution time  $t_{1,\text{opt}}$  in Eq. (22) or the qubit-probe coupling strength  $g$ . In this case, the QFI for the mixed initial probe  $\rho_0$  after the unitary evolution can be described by Eq. (9), i.e.,

$$\begin{aligned} F_Q &= F_{Q, +, \text{eff}} + F_{Q, -, \text{eff}} = \sum_{i=1}^d 4p_i \langle \psi_i | J_{\text{opt}}^2 | \psi_i \rangle \\ &\quad - \sum_{i,j=1}^d \frac{8p_i p_j}{p_i + p_j} | \langle \psi_i | e^{-i\pi J_z} J_{\text{opt}} | \psi_j \rangle |^2. \end{aligned} \quad (33)$$

When the second term in Eq. (33) vanishes, QFI can approach HL. For a pure state  $|\psi\rangle = |j, m\rangle_{\text{opt}}$  of the probe system, the operator  $e^{-i\pi J_z}$  plays the role of the spin-rotation around the  $z$ -axis with an angle  $\pi$  such that the second term becomes proportional



to  $|\langle\psi|e^{-i\pi J_z}J_{\text{opt}}|\psi\rangle|^2 = |\langle j, m|e^{-i\pi J_z}J_{\text{opt}}|j, m\rangle_{\text{opt}}|^2 = m^2|\langle j, m|j, -m\rangle_{\text{opt}}|^2 = 0$ . For a superposed state, e.g.,  $|\psi_m\rangle = a_m|j, m\rangle_{\text{opt}} + b_me^{-i\phi_m}|j, -m\rangle_{\text{opt}}$  with real numbers  $a_m$ ,  $b_m$ , and  $\phi_m$ , we have

$$|\langle\psi|e^{-i\pi J_z}J_{\text{opt}}|\psi\rangle|^2 = 4a_m^2b_m^2m^2\sin^2\phi_m. \quad (34)$$

It is found that the second term vanishes when  $\phi_m = n_3\pi$  with an integer  $n_3$  and hence  $F_Q = 4m^2$ . More generally, for a superposed state  $|\psi\rangle = \sum_m c_m|\psi_m\rangle$  with  $c_m$ 's the normalized complex numbers, Eq. (33) becomes

$$F_Q = 4\sum_m m^2|c_m|^2(1 - 4a_m^2b_m^2\sin^2\phi_m). \quad (35)$$

It is straightforward to find that  $F_Q = N^2$  of HL is attainable if and only if the probe state is prepared as  $|j, j\rangle_{\text{opt}}$ ,  $|j, -j\rangle_{\text{opt}}$ , or a superposed state over them, i.e.,  $a|j, j\rangle_{\text{opt}} + be^{-i\phi}|j, -j\rangle_{\text{opt}}$  with the phase  $\phi = n_3\pi$  and arbitrary real numbers  $a$  and  $b$ . It implies that in our protocol, the polarized states  $|j, j\rangle_{\text{opt}}$  and  $|j, -j\rangle_{\text{opt}}$  are of the optimized states for approaching HL in metrology precision besides the GHZ-like states. Inversely, any polarized state can become the optimized state for quantum metrology as long as one can construct the relevant collective angular momentum operator in Eq. (23) and circuit model in Fig. 1.

Equation (33) indicates the main advantage of our measurement-based metrology over the conventional parameter estimations [41–44] described by Eq. (9). The unconditional measurement on the ancillary qubit establishes a special effective phase generator, i.e.,  $\mathcal{H} = e^{-i\pi J_z}J_{\text{opt}}$ . In the absence of the ancillary qubit, i.e., on setting the coupling strength between the probe system and the ancillary qubit  $g = 0$ , Eq. (33) becomes

$$F_Q = \sum_{i=1}^d 4p_i\langle\psi_i|J_\phi^2|\psi_i\rangle - \sum_{i,j=1}^d \frac{8p_i p_j}{p_i + p_j} |\langle\psi_i|J_\phi|\psi_j\rangle|^2, \quad (36)$$

where the effective phase generator is  $J_\phi \equiv \cos(\phi)J_x - \sin(\phi)J_y$  with  $\phi = \omega_P t_1$ . In contrast to Eq. (33),  $F_Q = N^2$  is now attainable if and only if the probe is initialized as a GHZ state, i.e.,  $|\psi\rangle = (|j, j\rangle_\phi + e^{-i\phi_0}|j, -j\rangle_\phi)/\sqrt{2}$  with an arbitrary phase  $\phi_0$ . Here  $|j, m\rangle_\phi$  with  $-j \leq m \leq j$  are the eigenstates of the collective angular momentum operator  $J_\phi$ .

An asymptotic behavior to the Heisenberg scaling can appear even when the second term in Eq. (33) is partially eliminated under a mixed state. For example, one can suppose that the probe system is prepared as a thermal state in the bases of  $|j, m\rangle_{\text{opt}}$ , i.e.,

$$\rho_P^{\text{th}} = \sum_{m=-j}^j \frac{e^{-m\beta}}{Z_\beta} |j, m\rangle_{\text{opt}}\langle j, m|, \quad (37)$$

where  $Z_\beta = \text{Tr}[\exp(-\beta J_{\text{opt}})]$  is the partition function and  $\beta \equiv \omega_P/(k_B T)$  is the dimensionless inverse temperature.

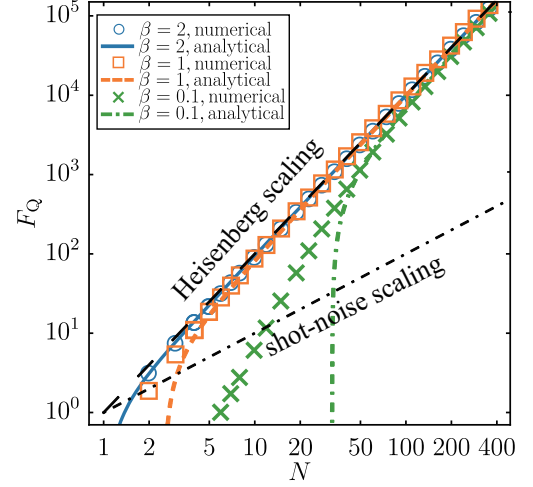


FIG. 2. QFI as a function of  $N$  for a thermal state  $\rho_P^{\text{th}}$ . The blue circles, orange squares, and green crosses indicate the exact numerical simulations in Eq. (38) with inverse temperature  $\beta = 2, 1$ , and  $0.1$ , respectively. The blue solid line, orange dashed line, and green dot-dashed line are the corresponding approximated analytical results by Eq. (39). The black-dashed line and the black dot-dashed line indicate the Heisenberg and shot-noise scalings, respectively. Here  $\rho_A = |+\rangle\langle +|$ ,  $t_1 = t_{1,\text{opt}}(n_1 = 0) = \pi/(2g)$ ,  $\omega_P = 10g$ , and  $\omega_A \approx 5g$ .

Then with  $d = N + 1 = 2j + 1$ ,  $p_m = e^{-m\beta}/Z_\beta$ , and  $|\psi_m\rangle_{\text{rangle}} = |j, m\rangle_{\text{opt}}$ , Eq. (33) becomes

$$\begin{aligned} F_Q &= \frac{4}{Z_\beta} \sum_{m=-j}^j m^2 e^{-m\beta} - \frac{8}{Z_\beta} \sum_{m=-j}^j \frac{m^2}{e^{-m\beta} + e^{m\beta}} \\ &\geq \frac{4 \sum_{m=-j}^j m^2 e^{-m\beta}}{\sum_{m=-j}^j e^{-m\beta}} - \frac{\pi^3}{\beta^3 \sum_{m=-j}^j e^{-m\beta}} \\ &= \frac{1}{(e^\beta - 1)^2} \left[ N^2 \frac{1 - e^{(3+N)\beta}}{1 - e^{(1+N)\beta}} + (N+2)^2 \frac{e^{2\beta} - e^{(1+N)\beta}}{1 - e^{(1+N)\beta}} \right. \\ &\quad \left. + (N^2 + 2N - 2) \frac{2e^{(2+N)\beta} - 2e^\beta}{1 - e^{(1+N)\beta}} \right] \\ &\quad - \frac{\pi^3}{\beta^3} \frac{e^{\frac{N\beta}{2}}(e^\beta - 1)}{e^{(N+1)\beta} - 1}, \end{aligned} \quad (38)$$

where we have used the inequality  $\sum_{m=-j}^j \frac{m^2}{e^{-m\beta} + e^{m\beta}} \leq \sum_{m=-\infty}^{\infty} \frac{m^2}{e^{-m\beta} + e^{m\beta}} \approx \int_{-\infty}^{\infty} dm \frac{m^2}{e^{-m\beta} + e^{m\beta}} = \pi^3/(8\beta^3)$ . Then for a large-size probe, i.e.,  $N \gg 1$ , it is approximated as

$$F_Q \geq N^2 - \frac{4}{e^\beta - 1} N + \frac{4(e^\beta + 1)}{(e^\beta - 1)^2} - \frac{\pi^3}{\beta^3} e^{-\frac{N\beta}{2}} (1 - e^{-\beta}). \quad (39)$$

Clearly,  $F_Q \rightarrow N^2$  when  $\beta \rightarrow \infty$ . It implies that the Heisenberg-scaling behavior dominates QFI at least in the low-temperature limit. The compact expression in Eq. (39) is confirmed to match with the numerical result in Fig. 2 and they both approach the Heisenberg scal-

ing for a sufficient large  $N$ . When  $\beta = 2$ ,  $\beta = 1$ , and  $\beta = 0.1$ , the approximated analytical results cannot be distinguished from the numerical simulation for  $N = 3$ ,  $N = 6$ , and  $N = 52$ , respectively. Even when  $\beta = 0.1$ , a high-temperature case, QFI becomes following the square scaling law for  $N > 120$ . With no loss of generality, we set  $\omega_P = 10g$  and  $\omega_A \approx 5g$  with  $n_2 = (9 - N)/2$ ,  $(10 - N)/2$  for odd and even  $N$ , respectively, according to Eq. (32).

## V. QUANTUM FISHER INFORMATION UNDER IMPRECISE CONTROL

The precise control over the joint evolution time  $t_1$  in Eq. (22) and the exact synchronization of the parametric encoding and the unconditional measurement on the ancillary qubit described by the whole unitary evolution in Eq. (16) are not strictly demanded in our protocol.

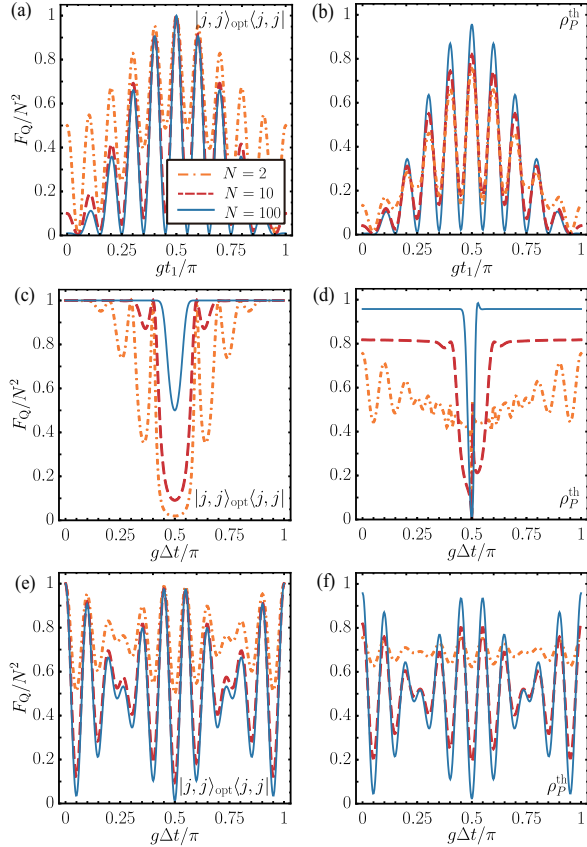


FIG. 3. Renormalized QFI  $F_Q/N^2$  for the probe state prepared as a polarized state  $\rho_P = |j, j\rangle_{\text{opt}}\langle j, j|$  [(a), (c), and (e)] or a thermal state  $\rho_P^{\text{th}}$  with  $\beta = 1$  [(b), (d), and (f)] with various probe-spin number  $N$ . (a) and (b):  $F_Q/N^2$  as a function of arbitrary periods  $gt_1$  of Evolution 1. (c) and (d):  $F_Q/N^2$  as a function of the measurement delay  $g\Delta t$  with a fixed and optimized  $gt_1 = \pi/2$ . (e) and (f):  $F_Q/N^2$  as a function of the parametric encoding delay  $g\Delta t$  with  $gt_1 = \pi/2$ . The other parameters are the same as Fig. 2.

With the ancillary-qubit state in Eq. (19) and the

probe state in Eq. (21), the unnormalized output state in Eq. (24) becomes

$$|\Psi_{\theta, \pm}\rangle = e^{-iHt_2} e^{-i\theta J_x} |\pm\rangle \langle \pm| e^{-iHt_1} |j, j\rangle_{\text{opt}} \otimes |+\rangle \quad (40)$$

under a general  $t_1$ , which can be normalized by the probability  $\mathcal{N}_{\pm} = [1 \pm \cos(2\omega_A t_1) \cos^N(gt_1)]/2$ . Through a similar calculation by Eq. (25), one can find that  $F_Q = N^2$  if and only if  $t_1 = t_{1, \text{opt}}$  given in Eq. (22).

This result can be confirmed by the numerical simulation over QFI as a function of the joint evolution time  $t_1$  in Figs. 3(a) and 3(b), where the probe (spin ensemble) is initialized as the polarized state  $\rho_P = |j, j\rangle_{\text{opt}}\langle j, j|$  and the thermal state  $\rho_P^{\text{th}}$  with  $\beta = 1$ , respectively. It is found that QFI presents a central-symmetrical pattern around the optimized point  $gt_1 = \pi/2$ . For the polarized state,  $F_Q$  reaches the peak value  $N^2$  when  $gt_1 = \pi/2$ , irrespective of the probe size  $N$ . For the thermal state,  $F_Q$  is proportional to  $N^2$  when  $gt_1 = \pi/2$  and the maximum value increases with  $N$ . In particular, we have  $F_Q/N^2 \approx 0.75, 0.82$ , and  $0.96$  for  $N = 2, 10$ , and  $100$ , respectively. For both polarized state and thermal state,  $F_Q$  attains a nearly periodical Heisenberg-scaling result when  $gt_1/\pi$  is around  $0.2, 0.3, 0.4, 0.6, 0.7$ , and  $0.8$ .

The synchronization of encoding and measurement is broken when a time delay presents between them. When the measurement falls behind the encoding with an interval  $\Delta t$ , the whole evolution operator of the circuit in Eq. (16) is modified to be

$$U_{\theta, \pm} = U(t_2) M_{\pm} U(\Delta t) R_x(\theta) U(t_{1, \text{opt}}) \\ = e^{-iHt_2} |\pm\rangle \langle \pm| e^{-iH\Delta t} e^{-i\theta J_x} e^{-iHt_{1, \text{opt}}}, \quad (41)$$

under the optimized  $t_1$  in Eq. (22). Consequently, the output state in Eq. (24) will be rewritten as

$$|\Psi_{\theta, \pm}\rangle = U_{\theta, \pm} |j, j\rangle_{\text{opt}} \otimes |+\rangle \\ = \frac{U(t_2)}{2} e^{-i(\omega_P + g)J_z \Delta t} [e^{-i\omega_A(\Delta t + t_{1, \text{opt}})} e^{-ij\theta} |j, j\rangle_x \\ \pm i^N e^{2igJ_z \Delta t} e^{i\omega_A(\Delta t + t_{1, \text{opt}})} e^{ij\theta} |j, -j\rangle_x] \otimes |\pm\rangle, \quad (42)$$

when the qubit is initialized as  $|\varphi\rangle_{\text{opt}} = |+\rangle$ . Analog to Eqs. (25) and (26), we have

$$F_Q = F_{Q, +, \text{eff}} + F_{Q, -, \text{eff}} \\ = \frac{N^2 [1 - \sin^{2N}(g\Delta t)]}{1 - \sin^{2N}(g\Delta t) \cos^2[2\omega_A(\Delta t + t_{1, \text{opt}}) + N\theta]}. \quad (43)$$

This expression indicates that QFI turns out to be relevant to the to-be-estimated phase  $\theta$ . Generally for a large-size probe, i.e.,  $N \gg 1$ , the dependence of QFI on  $\theta$  vanishes and Eq. (43) can be approximated as  $F_Q \approx N^2$  when  $|\sin(g\Delta t)| < 1$ . Without loss of generality, we set  $\theta \approx 0$  and show the dependence of QFI on the time delay  $\Delta t$  of measurement under various probe size  $N$  in Fig. 3(c) for the polarized state of probe. One can find that the quantum Fisher information tends to maintain its maximum value  $N^2$  in a wider regime of  $\Delta t$  for a larger

probe size  $N$ , as illustrated by Eq. (43). It indicates that a large probe can significantly reduce its sensitivity to the imprecise control over the measurement moment. This reduction still holds when the probe starts from a thermal state, as shown in Fig. 3(d).

As for the nonvanishing encoding delay, i.e., the parametric encoding falls behind the measurement with an interval  $\Delta t$ , the whole evolution operator in Eq. (16) becomes

$$U_{\theta,\pm} = U(t_2)R_x(\theta)U(\Delta t)M_{\pm}U(t_{1,\text{opt}}) \\ = e^{-iHt_2}e^{-i\theta J_x}e^{-iH\Delta t}|\pm\rangle\langle\pm|e^{-iHt_{1,\text{opt}}}. \quad (44)$$

when the other conditions are invariant.

Upon the optimal input states in Eqs. (19) and (21), Eq. (24) is now rewritten as

$$|\Psi_{\theta,\pm}\rangle = U_{\theta,\pm}|j,j\rangle_{\text{opt}} \otimes |+\rangle \\ = \frac{U(t_2)}{2}R_x(\theta)U(\Delta t)e^{-i\omega_A t_{1,\text{opt}}} \\ \times (\mathcal{I}^{N+1} \pm e^{2i(\omega_A + gJ_z)t_{1,\text{opt}}})|j,j\rangle_x \otimes |\pm\rangle, \quad (45)$$

with a fixed probability  $\mathcal{N}_{\theta,\pm} = 1/2$ . Consequently, the effective QFI is

$$F_Q = F_{Q,+,\text{eff}} + F_{Q,-,\text{eff}} \\ = \frac{N}{4}\{2(N+1) + (N-1) \\ \times [\cos(2\Delta t(g - \omega_P)) + \cos(2\Delta t(g + \omega_P))]\}. \quad (46)$$

It is consistent with Eq. (26) that  $F_Q = N^2$  when  $\Delta t = 0$ . When  $\Delta t \ll 1$ , we have

$$F_Q \approx N^2 - N(N-1)(g^2 + \omega_P^2)\Delta t^2, \quad (47)$$

up to the second order of  $\Delta t$ . Again this result confirms that our condition about the joint evolution time  $t_1$  in Eq. (22) is optimal. In Figs. 3(e) and 3(f), we show the dependence of the  $F_Q$  on the encoding delay  $\Delta t$  for the polarized probe state and the thermal probe state, respectively, under a proper ancillary qubit state and the optimal evolution time  $t_1$  in Eqs. (19) and (22). Both of them demonstrate that the detrimental effect from the encoding decay on QFI is periodically presented. The Heisenberg scaling appears when  $g\Delta t = n\pi$  with an integer  $n$  for various  $N$ .

## VI. CLASSICAL FISHER INFORMATION

In a practical scenario of parametric estimation, CFI measures the amount of information that can be extracted from the probability distribution for the output state [45–47], which is upper bounded by QFI about the metrology precision. In this section, we derive CFI of our protocol under the same settings as those for QFI in Fig. 2, i.e., the optimized joint-evolution time  $t_{1,\text{opt}}$ , and an optimal state of the probe system  $|j,j\rangle_{\text{opt}}$ , and the

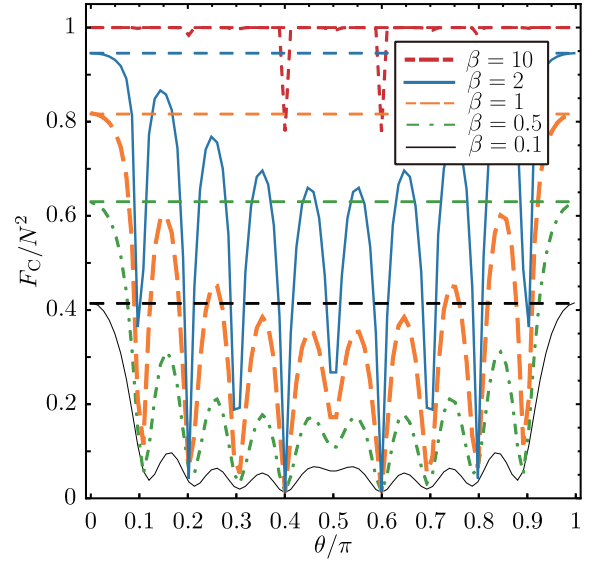


FIG. 4. Renormalized CFI  $F_C/N^2$  as a function of the to-be-estimated phase  $\theta$  for the probe state prepared as a thermal state  $\rho_P^{\text{th}}$  with various  $\beta$ . The dashed horizontal lines indicate the corresponding renormalized QFI  $F_Q/N^2$ . The ancillary qubit is initialized as  $\rho_A = |+\rangle\langle+|$ . The probe size is  $N = 10$ . The other parameters are the same as Fig. 2.

ancillary qubit  $|\varphi\rangle_{\text{opt}}$  in Eq. (22) with  $n_1 = 0$ , Eq. (21), and Eq. (19), respectively.

The probe state after the three-stage evolution as described by the evolution operator (16) reads

$$\rho_{\pm}(\theta) = \text{Tr}_A[U_{\theta,\pm}\rho_P \otimes |+\rangle\langle+|U_{\theta,\pm}^\dagger] \\ = \frac{1}{2}\text{Tr}_A\{U(t_2)[|j,j\rangle_x\langle j,j| + |j,-j\rangle_x\langle j,-j| \\ \pm e^{-i\Phi}|j,j\rangle_x\langle j,-j| \pm e^{i\Phi}|j,-j\rangle_x\langle j,j|] \\ \otimes |\pm\rangle\langle\pm|U^\dagger(t_2)\}, \quad (48)$$

with the normalization coefficient  $\mathcal{N}_{\theta,\pm} = 1/2$  and the phase parameter  $\Phi \equiv 2\omega_A t_{1,\text{opt}} + N\theta + \frac{N\pi}{2}$ . Subsequently, one can perform the projective measurements  $|j,m\rangle$  on the probe system as the last operation of the circuit model in Fig. 1, where  $|j,m\rangle$  denote the eigenstate of the collective spin operators  $J_z$  with eigenvalue  $m$ . The probability of detecting the probe state in the state  $|j,m\rangle$  and its first derivative with respect to the to-be-estimated phase  $\theta$  read

$$P(m,\pm|\theta) = \langle j,m|\rho_{\pm}(\theta)|j,m\rangle \\ = \frac{1}{2}[|\langle j,m|j,j\rangle_x|^2 \pm (-i)^{2(j+m)}\cos(\Phi)|\langle j,m|j,j\rangle_x|^2], \\ \partial_\theta P(m,\pm|\theta) = \mp \frac{(-i)^{2(j+m)}N}{2}\sin(\Phi)|\langle j,m|j,j\rangle_x|^2, \quad (49)$$

respectively. Consequently, we have

$$\begin{aligned} \frac{[\partial_\theta P(m, \pm|\theta)]^2}{P(m, \pm|\theta)} &= \frac{N^2}{2} \frac{\sin^2(\Phi) |\langle j, m|j, j \rangle_x|^2}{1 \pm (-i)^{2(j+m)} \cos(\Phi)} \\ &= \frac{N^2}{2} [1 \mp i^{2(j-m)} \cos(\Phi)] |\langle j, m|j, j \rangle_x|^2. \end{aligned} \quad (50)$$

In the proceeding two steps, we have used the identities

$$\begin{aligned} \langle j, m|j, -j \rangle_x &= (-i)^{2(j+m)} \langle j, m|j, j \rangle_x, \\ \sin^2(\Phi) &= [1 \pm (-i)^{2(j+m)} \cos(\Phi)][1 \mp i^{2(j-m)} \cos(\Phi)]. \end{aligned} \quad (51)$$

Substituting Eq. (50) to Eq. (1), we have

$$\begin{aligned} F_C &= \sum_{m=-j}^j \left( \frac{[\partial_\theta P(m, +|\theta)]^2}{P(m, +|\theta)} + \frac{[\partial_\theta P(m, -|\theta)]^2}{P(m, -|\theta)} \right) \\ &= N^2 \sum_{m=-j}^j |\langle j, m|j, j \rangle_x|^2 = N^2 = F_Q. \end{aligned} \quad (52)$$

The last line is exactly the same as Eq. (26), irrespective of the idle evolution time  $t_2$ . The derivation also applies to  $|j, -j\rangle_{\text{opt}}$  and  $a|j, j\rangle_{\text{opt}} + be^{-i\phi}|j, -j\rangle_{\text{opt}}$ . It is thus verified that in our protocol CFI can saturate with its quantum counterpart as long as the probe is prepared into the optimized state.

In Fig. 4, we plot the renormalized CFI  $F_C/N^2$  as a function of the to-be-estimated parameter  $\theta$  for the thermal state  $\rho_P^{\text{th}}$  with a fixed probe spin number  $N = 10$  and various  $\beta$ . It is found that, in the high-temperature limit, i.e.,  $\beta \rightarrow 0$ , the classical Fisher information is much lower than the quantum Fisher information (see the lowest horizontal line for  $\beta = 0.1$ ), except when  $\theta$  is around 0 and  $\pi$ . On the contrary, in the low-temperature limit (see the highest horizontal line), e.g.,  $\beta = 10$ , CFI can saturate with its quantum counterpart in almost the full

regime of  $\theta$ . In addition, the upperbound of CFI is found to be  $F_C/N^2 = 0.415, 0.628, 0.818, 0.946$ , and almost unit for  $\beta = 0.1, 0.5, 1, 2$ , and 10.

## VII. CONCLUSION

In summery, we introduce the unconditional measurement on an ancillary system as a resource to replace those popularly used in conventional quantum metrology protocols based on large-spin or spin-ensemble systems, e.g. the initial GHZ-like state or nonlinear Hamiltonian. In our measurement-based metrology protocol, the polarized states and their superposition of an optimized collective angular momentum operator can be used to exactly achieve the Heisenberg-scaling behavior in parameter estimation with respect to the probe size  $N$ . Our protocol even allows the probe system prepared at the thermal state to follow an asymptotic square scaling law of metrology if  $N$  becomes sufficiently large. The metrology precision by our protocol can be optimized under the precise control over the joint evolution time of probe and ancillary qubit before the exact synchronization of the parametric encoding and the unconditional measurement on the qubit. Yet the numerical simulation shows that it is not sensitive to the fluctuation of the joint evolution time and the time delay between encoding and measurement. Last but not least, by virtue of the projective measurement on the probe system, the classical Fisher information in our protocol can saturate its quantum counterpart, irrespective of the idle evolution time after the parametric encoding. In essence, the developed protocol proves that both GHZ-like state and nonlinear Hamiltonian are not necessary conditions to achieve the Heisenberg-scaling metrology. We can have a more economical way, e.g., applying a nearly classical state, to achieve that.

- 
- [1] Z. Sun, J. Ma, X.-M. Lu, and X.-G. Wang, *Fisher information in a quantum-critical environment*, *Phys. Rev. A* **82**, 022306 (2010).
  - [2] J. Ma, Y.-X. Huang, X.-G. Wang, and C. P. Sun, *Quantum fisher information of the greenberger-horne-zeilinger state in decoherence channels*, *Phys. Rev. A* **84**, 022302 (2011).
  - [3] M. G. Genoni, S. Olivares, D. Brivio, S. Cialdi, D. Cipriani, A. Santamato, S. Vezzoli, and M. G. A. Paris, *Optical interferometry in the presence of large phase diffusion*, *Phys. Rev. A* **85**, 043817 (2012).
  - [4] B. M. Escher, L. Davidovich, N. Zagury, and R. L. de Matos Filho, *Quantum metrological limits via a variational approach*, *Phys. Rev. Lett.* **109**, 190404 (2012).
  - [5] W. Zhong, Z. Sun, J. Ma, X. Wang, and F. Nori, *Fisher information under decoherence in bloch representation*, *Phys. Rev. A* **87**, 022337 (2013).
  - [6] V. Giovannetti, S. Lloyd, and L. Maccone, *Quantum-enhanced measurements: beating the standard quantum limit*, *Science* **306**, 1330 (2004).
  - [7] S. M. Kay, *Fundamentals of statistical signal processing: estimation theory* (Prentice-Hall, Inc., 1993).
  - [8] A. D. Ludlow, M. M. Boyd, J. Ye, E. Peik, and P. O. Schmidt, *Optical atomic clocks*, *Rev. Mod. Phys.* **87**, 637 (2015).
  - [9] H. Katori, *Optical lattice clocks and quantum metrology*, *Nat. Photonics* **5**, 203 (2011).
  - [10] C. M. Caves, *Quantum-mechanical noise in an interferometer*, *Phys. Rev. D* **23**, 1693 (1981).
  - [11] M. A. Taylor and W. P. Bowen, *Quantum metrology and its application in biology*, *Phys. Rep.* **615**, 1 (2016).
  - [12] N. Mauranyapin, L. Madsen, M. Taylor, M. Waleed, and W. Bowen, *Evanescent single-molecule biosensing with quantum-limited precision*, *Nat. Photonics* **11**, 477 (2017).



- [13] J. A. Jones, S. D. Karlen, J. Fitzsimons, A. Ardavan, S. C. Benjamin, G. A. D. Briggs, and J. J. Morton, *Magnetic field sensing beyond the standard quantum limit using 10-spin noon states*, *Science* **324**, 1166 (2009).
- [14] C. Song, K. Xu, H.-K. Li, Y.-R. Zhang, X. Zhang, W.-X. Liu, Q.-J. Guo, Z. Wang, W.-H. Ren, J. Hao, *et al.*, *Generation of multicomponent atomic schrödinger cat states of up to 20 qubits*, *Science* **365**, 574 (2019).
- [15] T. Choi, S. Debnath, T. A. Manning, C. Figgatt, Z.-X. Gong, L.-M. Duan, and C. Monroe, *Optimal quantum control of multimode couplings between trapped ion qubits for scalable entanglement*, *Phys. Rev. Lett.* **112**, 190502 (2014).
- [16] R. Barends, J. Kelly, A. Megrant, A. Veitia, D. Sank, E. Jeffrey, T. C. White, J. Mutus, A. G. Fowler, B. Campbell, *et al.*, *Superconducting quantum circuits at the surface code threshold for fault tolerance*, *Nature* **508**, 500 (2014).
- [17] H. Kaufmann, T. Ruster, C. T. Schmiegelow, M. A. Luda, V. Kaushal, J. Schulz, D. Von Lindenfels, F. Schmidt-Kaler, and U. Poschinger, *Scalable creation of long-lived multipartite entanglement*, *Physical review letters* **119**, 150503 (2017).
- [18] M. Kitagawa and M. Ueda, *Squeezed spin states*, *Phys. Rev. A* **47**, 5138 (1993).
- [19] A. Sørensen, L.-M. Duan, J. I. Cirac, and P. Zoller, *Many-particle entanglement with bose-einstein condensates*, *Nature* **409**, 63 (2001).
- [20] L. Pezzé and A. Smerzi, *Entanglement, nonlinear dynamics, and the heisenberg limit*, *Phys. Rev. Lett.* **102**, 100401 (2009).
- [21] G. S. Agarwal, R. R. Puri, and R. P. Singh, *Atomic schrödinger cat states*, *Phys. Rev. A* **56**, 2249 (1997).
- [22] D. Leibfried, E. Knill, S. Seidelin, J. Britton, R. B. Blakestad, J. Chiaverini, D. B. Hume, W. M. Itano, J. D. Jost, C. Langer, *et al.*, *Creation of a six-atom 'schrödinger cat' state*, *Nature* **438**, 639 (2005).
- [23] B. Alexander, J. J. Bollinger, and H. Uys, *Generating greenberger-horne-zeilinger states with squeezing and postselection*, *Phys. Rev. A* **101**, 062303 (2020).
- [24] Y. Huang and M. Moore, *Creation, detection, and decoherence of macroscopic quantum superposition states in double-well bose-einstein condensates*, *Phys. Rev. A* **73**, 023606 (2006).
- [25] H. Cramér, *Mathematical methods of statistics*, Vol. 26 (Princeton university press, 1999).
- [26] S. L. Braunstein and C. M. Caves, *Statistical distance and the geometry of quantum states*, *Phys. Rev. Lett.* **72**, 3439 (1994).
- [27] S. L. Braunstein, C. M. Caves, and G. J. Milburn, *Generalized uncertainty relations: theory, examples, and lorentz invariance*, *Ann. Phys.* **247**, 135 (1996).
- [28] Y.-M. Zhang, X.-W. Li, W. Yang, and G.-R. Jin, *Quantum fisher information of entangled coherent states in the presence of photon loss*, *Phys. Rev. A* **88**, 043832 (2013).
- [29] J. Liu, X.-X. Jing, W. Zhong, and X.-G. Wang, *Quantum fisher information for density matrices with arbitrary ranks*, *Commun. Theor. Phys.* **61**, 45 (2014).
- [30] D. C. Brody and E.-M. Graefe, *Mixed-state evolution in the presence of gain and loss*, *Phys. Rev. Lett.* **109**, 230405 (2012).
- [31] V. Giovannetti, S. Lloyd, and L. Maccone, *Quantum metrology*, *Phys. Rev. Lett.* **96**, 010401 (2006).
- [32] S. Pang and T. A. Brun, *Quantum metrology for a general hamiltonian parameter*, *Phys. Rev. A* **90**, 022117 (2014).
- [33] V. B. Braginsky and F. Y. Khalili, *Quantum non-demolition measurements: the route from toys to tools*, *Rev. Mod. Phys.* **68**, 1 (1996).
- [34] K. Hammerer, A. S. Sørensen, and E. S. Polzik, *Quantum interface between light and atomic ensembles*, *Rev. Mod. Phys.* **82**, 1041 (2010).
- [35] T. Pellizzari, S. A. Gardiner, J. I. Cirac, and P. Zoller, *Decoherence, continuous observation, and quantum computing: A cavity qed model*, *Phys. Rev. Lett.* **75**, 3788 (1995).
- [36] A. N. Pyrkov and T. Byrnes, *Entanglement generation in quantum networks of bose-einstein condensates*, *New J. Phys.* **15**, 093019 (2013).
- [37] G. Gillard, E. Clarke, and E. A. Chekhovich, *Harnessing many-body spin environment for long coherence storage and high-fidelity single-shot qubit readout*, *Nat. Commun.* **13**, 4048 (2022).
- [38] V. Meyer, M. A. Rowe, D. Kielpinski, C. A. Sackett, W. M. Itano, C. Monroe, and D. J. Wineland, *Experimental demonstration of entanglement-enhanced rotation angle estimation using trapped ions*, *Phys. Rev. Lett.* **86**, 5870 (2001).
- [39] C. Gross, T. Zibold, E. Nicklas, J. Esteve, and M. K. Oberthaler, *Nonlinear atom interferometer surpasses classical precision limit*, *Nature* **464**, 1165 (2010).
- [40] C. F. Ockeloen, R. Schmied, M. F. Riedel, and P. Treutlein, *Quantum metrology with a scanning probe atom interferometer*, *Phys. Rev. Lett.* **111**, 143001 (2013).
- [41] V. Giovannetti, S. Lloyd, and L. Maccone, *Advances in quantum metrology*, *Nat. Photonics* **5**, 222 (2011).
- [42] G. Tóth and I. Apellaniz, *Quantum metrology from a quantum information science perspective*, *J. Phys. A: Math. Theor.* **47**, 424006 (2014).
- [43] W. Nawrocki, *Introduction to quantum metrology*, 2nd ed. (Springer Nature Switzerland, Cham, Switzerland, 2019).
- [44] E. Polino, M. Valeri, N. Spagnolo, and F. Sciarrino, *Photonic quantum metrology*, *AVS Quantum Sci.* **2**, 024703 (2020).
- [45] D. Braun, G. Adesso, F. Benatti, R. Floreanini, U. Marzolino, M. W. Mitchell, and S. Pirandola, *Quantum-enhanced measurements without entanglement*, *Rev. Mod. Phys.* **90**, 035006 (2018).
- [46] J. Liu, H.-D. Yuan, X.-M. Lu, and X.-G. Wang, *Quantum fisher information matrix and multiparameter estimation*, *J. Phys. A: Math. Theor.* **53**, 023001 (2020).
- [47] K. C. Tan, V. Narasimhachar, and B. Regula, *Fisher information universally identifies quantum resources*, *Phys. Rev. Lett.* **127**, 200402 (2021).